Anal Bioanal Chem (2012) 403:2339–2351
DOI 10.1007/s00216-012-6025-4

ORIGINAL PAPER

Fluorescence recovery after photobleaching reveals the biochemistry of nucleocytoplasmic exchange

Ranieri Bizzarri · Francesco Cardarelli · Michela Serresi · Fabio Beltram

Received: 9 December 2011 / Revised: 19 March 2012 / Accepted: 4 April 2012 / Published online: 15 May 2012
© Springer-Verlag 2012

Abstract Fluorescence recovery after photobleaching (FRAP) can help unveil subtle dynamical and biochemical properties of intracellular components. A peculiar aspect of this method is that it is based on the change of optical properties only, whereas dynamics and biochemistry of the molecules of interest are not perturbed. This makes FRAP particularly suitable for the study of protein translocation, e.g., between nucleus and cytoplasm. Here we present a comprehensive theoretical treatment of FRAP applied to protein nucleocytoplasmic translocation by passive diffusion and/or energy-driven processes across the nuclear envelope. Our mathematical model is validated by experimental FRAP studies with functionalized fluorescent protein chimeras. Using this approach we demonstrate that molecular crowding at the nuclear pore does not hamper passive diffusion and calculate the dimension of the nuclear pore size (5.33 nm). Additionally, our FRAP analysis reveals the biochemical parameters (maximum translocation rate and dissociation constant of the transport complex in cytoplasm) associated with the active import of a prototypical nuclear localization sequence (NLS of SV40) and related mutants. We demonstrate that transportin binding and active import into the nucleus are independent processes that can be separately modulated. The present results are discussed in light of their potential to help in engineering sequences for intracellular targeted delivery of sensors and/or therapeutic compounds. Finally, the limits of validity of our mathematical model are addressed.

Keywords Fluorescence/Luminescence · Kinetics · Optical sensors · Biological samples · Bioanalytical methods

Published in the special issue *Young Investigators in Analytical and Bioanalytical Science* with guest editors S. Daunert, J. Bettmer, T. Hasegawa, Q. Wang and Y. Wei.

R. Bizzarri (✉) · F. Beltram
NEST, Scuola Normale
Superiore and Istituto Nanoscienze – CNR,
Piazza San Silvestro 12,
56127 Pisa, Italy
e-mail: r.bizzarri@sns.it

F. Cardarelli · M. Serresi · F. Beltram
Center for Nanotechnology Innovation
@ NEST, Istituto Italiano di Tecnologia,
Piazza San Silvestro 12,
56127 Pisa, Italy

Present Address:
R. Bizzarri
Istituto di Biofisica – CNR,
via Moruzzi 1,
56124 Pisa, Italy

Ranieri Bizzarri received his PhD in Chemistry from Scuola Normale Superiore (SNS), Pisa, Italy. He is currently a researcher at the Biophysics Institute of the Italian National Research Council. He was a visiting scientist at Cornell University (USA), CNRS—Université de Paris XII (France), and Twente University (the Netherlands). His scientific interests mainly concern the development of fluorescent probes and related imaging techniques to report on biochemical processes in living cells.

Introduction

Fluorescence recovery after photobleaching (FRAP) is a microscopy protocol remarkably suited to study the mobility of molecules and particles [1]. In a FRAP experiment, a

short and intense light beam is applied to irreversibly photobleach fluorescent molecules in a micron- or submicron-size region of the sample. After photobleaching, the "dark" molecules gradually transfer out of the photobleached area, while at the same time unbleached molecules enter it from the surroundings. This exchange leads to a recovery of fluorescence within the photobleached area (and to the loss of fluorescence in the surroundings) that can be monitored by low-intensity excitation. Analysis of the recovery curves by means of a suitable biophysical model yields insight into the translocation dynamics of the molecule under study.

FRAP was originally conceived in 1974 by Peters [2]. Nonetheless, this technique owes much of its relevance to the discovery and development of autofluorescent proteins (FPs) [3], a class of genetically encodable fluorescent molecules derived from sea organisms such as jellyfish or corals. The development of FPs gave access to a virtually unlimited number of fluorescent constructs that can be expressed intracellularly and whose dynamical properties can be investigated by FRAP. FP-based FRAP was successfully applied to many scientific fields, including biophysics and biomedicine, at cellular and subcellular level [4–8]. It is worth noting that another critical factor in the implementation of the FRAP technique was the recent development of microscopy setups that allow high-resolution imaging on living cells [9].

Among the dynamical cases amenable to FRAP analysis, a particularly interesting situation occurs when diffusion takes place between two (or more) compartments separated by a permeable membrane, a situation often encountered in biological systems where membrane compartmentalization is at the basis of life. Molecular diffusion through the nuclear membrane (called nuclear envelope, NE) falls into this class. In eukaryotes, the NE plays a primary functional role because it mediates the exchange of regulative and instructive molecules between the nucleus and the cytoplasm. Hence, the regulation of NE permeability is a powerful mechanism to control cell life and represents a very significant subject for FRAP biological investigations [10–12].

Nucleocytoplasmic shuttling ordinarily takes place through the nuclear pore complex (NPC), a 125-MDa protein complex inserted in the NE containing up to 30 distinct types of proteins arranged with an octagonal-symmetry cylindrical structure around the axis of transport and a planar pseudosymmetry through the NE [11]. Molecular diffusion through the nuclear pore is restricted on the basis of size and the presence or absence of specific recognition motifs [13]. Molecules up to 60–70 kDa can penetrate the NE from either side in the absence of a signaling sequence, a mechanism called *passive diffusion* [14]. Passive diffusion is fast for small molecules, but becomes very inefficient as the upper molecular weight limit is approached, thus leading to size-dependent permeation characteristics [15, 16]. In contrast, *facilitated translocation* allows the passage of complexes as large as several megadaltons, provided these aggregates carry molecular motifs selectively recognized by a group of transport proteins [17]. The recognition motifs that drive the molecule towards the nucleus are called nuclear localization signals (NLS) and the related transport proteins are named *importins*. Similarly, we speak of nuclear export signals (NES) and *exportins*. Importins and exportins mediate the interaction with (or are part of) the NPC and modulate its permeability characteristics [18]. This process is coupled to an input of metabolic energy, which permits transport against a gradient of chemical potential [19]. This is usually referred to as *active transport*: energy deprivation leads to the blockage of facilitated translocation and is a typical assay to identify importin- or exportin-mediated NE crossing [20].

In this article we shall present a simple yet comprehensive approach developed from our recent studies on active/passive transport of cell-penetrating peptides [21, 22]. Our approach combines an experimental system based on GFP-modified cargoes with a theoretical model of nucleocytoplasmic translocation that constitutively accounts for the presence of binding reactions and molecular complexes of the diffusing species. On this basis, we shall argue that FRAP experiments stand out as a time-resolved technique perfectly tailored to the quantitative investigation of passive and active nucleocytoplasmic translocation of specific cargoes.

FRAP theory of nucleocytoplasmic translocation

Before describing our mathematical model of FRAP applied to nucleocytoplasmic translocation, a relevant point of the FRAP technique has to be stressed: *bleaching neither modifies the diffusion properties of any molecule nor does it introduce a molecular gradient of any sort; bleaching only shuts off the optical response of the fluorescent "label"*. Yet, FRAP witnesses a diffusion process. This apparent contradiction is easily solved by noting that diffusion is ruled by a linear equation (Fick's 1st law)

$$\vec{J} = -D \cdot \nabla C(x,y,z) \tag{1}$$

where $\vec{J}$ is the diffusion flux, $C(x,y,z)$ is the concentration at each point, and D is the diffusion coefficient of the molecule under observation, generally measured in cm^2/s or $\mu m^2/s$. Such linearity allows for the decomposition of the original diffusion system into a sum of arbitrary molecular subsets, each one equivalent to the global system in terms of its diffusion properties. These subsets can be distinguished by diffusion-unrelated properties, including fluorescence

emission. The subsets constituted by unbleached (emissive) and bleached (non-emissive) molecules are both of relevance in FRAP. Fick's 1st law is not violated if the spatially localized bleaching step introduces spatial gradients into the emissive and bleached subsets, *because the net sum of these subgradients is zero*; remarkably, we are able to follow the diffusion of the sole "emissive" subset on account of the fluorescence property of its molecular components.

The same consideration holds when the molecules under observation participate in any other process unrelated to their optical properties: photobleaching introduces *chemical gradients in the emissive and non-emissive subsets*, but, overall, the system is at equilibrium (or at steady state) in relation to the process under consideration (e.g., protein binding).

In our model of nucleus–cytoplasm exchange, two mechanisms account for molecular transport across the NE: passive diffusion and active transport. There is much evidence that these two processes are independent [13] and we shall decouple them completely in terms of analytical equations describing the molecular fluxes. Nucleus and cytoplasm are supposed to be two well-mixed compartments, i.e., we shall assume that intracompartment diffusion is much faster than active or passive diffusion across the NE. In the last section of the paper we discuss the range of validity of this assumption in terms of molecular dimensions of the cargo under study. Also, we shall suppose that no changes in the global concentration of the molecular players take place during the FRAP measurement. This means that any biochemical process involving the diffusing moiety is at equilibrium or at *steady state*. This assumption is justified by the longer timescale of protein expression and folding (hours) compared to the FRAP experiment (seconds, minutes).

Passive diffusion

The NE is modeled as a two-way permeable membrane with a resistivity dependent on the molecular weight of the diffusing molecule. For a diffusing molecule X crossing a membrane, Renkin implemented Fick's 1st law by means of experimental data, obtaining the empirical equation [23]

$$J_X^p = N_p A_p D_X \cdot \frac{([X]_C - [X]_N)}{L} \cdot f(r_X, r_p) \tag{2}$$

where J_X^p (mol/s) is the *surface-integrated* passive molar flux of X between the two compartments (considered positive when it is from cytoplasm to nucleoplasm, negative otherwise), N_p is the total number of pores present on the NE, A_p is the geometrical pore area, D_X is the diffusion coefficient of X, L is the effective length of the pores connecting the nucleus to the cytoplasm, and $[X]_C$ and $[X]_N$ are the concentrations of emissive X in the cytoplasm and nucleus, respectively. In our notation $[X]_C^0$ and $[X]_N^0$ represent the prebleach concentrations of X in cytoplasm and nucleus, respectively; $[X]_C^0$ and $[X]_N^0$ correspond to global concentrations of X (emissive+bleached). According to Renkin's theory, the diffusion of molecules through cylindrical pores with nanometer radii is restricted by both steric hindrance at the pore aperture and viscous drag inside the pore. These effects are taken into account in Eq. 2 by the factor $f(r_X, r_p)$, which is an empirical function of the radii of both X and the pore (r_X r_p).

Active transport

Active transport is easily accounted for by considering two (surface-integrated) diffusion fluxes of X, one from cytoplasm to the nucleus, $J_X^{C\to N}$, and one with the opposite direction, $J_X^{N\to C}$. These fluxes are directly proportional to the fraction of X molecules engaged in a complex with the import and/or export machinery in each compartment

$$J_X^{C\to N} = \nu_{C\to N} \cdot \chi_C \cdot [X]_C^0 \tag{3a}$$

$$J_X^{N\to C} = -\nu_{N\to C} \cdot \chi_N \cdot [X]_N^0 \tag{3b}$$

where χ_C and χ_N are the fractions of X *bound to* the transport machinery in the cytoplasm and the nucleoplasm, respectively. Fluxes are considered positive when directed towards the nucleus and negative otherwise. All kinetic features of importin- and exportin-promoted transport are gathered into the rate constants $\nu_{C\to N}$ and $\nu_{N\to C}$, respectively. Notably, $\nu_{C\to N}$ and $\nu_{N\to C}$ are constant within the timescale relevant to FRAP experiments (seconds to a few minutes), on account of our assumption of global equilibrium or steady state with respect to all the intracellular processes relevant to nucleocytoplasmic diffusion.

Equations 3a, b refer to *overall* fluxes of X molecules (i.e., emissive+bleached). When only emissive molecules are to be considered, flux expressions have to be changed to take into account the probability that the transport machinery will shuttle a fluorescent molecule; this probability is expressed by the ratio of fluorescent molecules over their total concentration, yielding

$$J_X^{C\to N} = \nu_{C\to N} \cdot \chi_C \cdot [X]_C^0 \cdot \frac{[X]_C}{[X]_C^0} = \nu_{C\to N} \cdot \chi_C \cdot [X]_C \tag{4a}$$

$$J_X^{N\to C} = -\nu_{N\to C} \cdot \chi_N \cdot [X]_N^0 \cdot \frac{[X]_N}{[X]_N^0} = -\nu_{N\to C} \cdot \chi_N \cdot [X]_N \tag{4b}$$

Hereafter, $J_X^{C\to N}$ and $J_X^{N\to C}$ will denote active fluxes of unbleached molecules, the latter being the only subject of FRAP analysis.

Comprehensive model of fluorescent molecule diffusion

A comprehensive set of differential equations accounting for the diffusion of fluorescent molecules across the NE can be written summing up the single contributes expressed by passive (Eq. 2) and active (Eq. 4a, b) fluxes, and remembering that the surface-integrated flux of X between the two compartments can be written as

$$J_X = \left(J_X^p + J_X^{C\to N} - J_X^{N\to C}\right) = V_N \cdot \frac{d[X]_N}{dt} = -V_C \cdot \frac{d[X]_C}{dt} \tag{5}$$

where V_C and V_N are cytoplasm and nuclear volumes, respectively. We have

$$\frac{d[X]_C}{dt} = \frac{-\left[\alpha_C P_X + k_X^{C\to N}\right]\cdot [X]_C + \left[\alpha_N P_X + k_X^{N\to C}\right]\cdot [X]_N}{V_C} \tag{6a}$$

$$\frac{d[X]_N}{dt} = \frac{\left[\alpha_C P_X + k_X^{C\to N}\right]\cdot [X]_C - \left[\alpha_N P_X + k_X^{N\to C}\right]\cdot [X]_N}{V_N} \tag{6b}$$

where (see Eqs. 2 and 4a, b)

$$P_X = \frac{N_p A_p D_X}{L}\cdot f\left(r_X, r_p\right) \tag{7}$$

$$k_X^{C\to N} = \nu_{C\to N}\cdot \chi_C \text{ and } k_X^{N\to C} = \nu_{N\to C}\cdot \chi_N \tag{8}$$

Parameters $P_X, k_X^{C\to N}, k_X^{N\to C}$ have dimensions $\mu m^3/s$ and are called the permeability coefficients of passive and active C→N and N→C diffusion, respectively. The scaling factors α_C and α_N take into account the possibility that the *actual* passive permeation of X is different on either side of the NE owing to binding interaction with local moieties (otherwise $\alpha_C=\alpha_N=1$).

Notably, our analysis leads to a system of differential equations (Eq. 6a, b) whose variables are the concentrations of fluorescent X in each compartment. The system solution is represented by a set of two monoexponential functions

$$[X]_C(t) = [X]_C^\infty + \left([X]_C^0 - [X]_C^\infty\right)\cdot \exp(-t/\tau) \tag{9a}$$

$$[X]_N(t) = [X]_N^\infty + \left([X]_N^0 - [X]_N^\infty\right)\cdot \exp(-t/\tau) \tag{9b}$$

where τ is the time constant of concentration recovery/depletion, and $[X]_C^\infty$ and $[X]_N^\infty$ represent the concentration of X in the cytoplasm and in the nucleoplasm when the diffusion process is terminated (*equilibrium state*), respectively. If we define the nuclear to cytoplasmic concentration ratio at equilibrium as $K_{eq} = [X]_N^\infty / [X]_C^\infty$, it is easy to show that the following relations hold:

$$K_{eq} = \frac{\alpha_C P_X + k_X^{C\to N}}{\alpha_N P_X + k_X^{N\to C}} \tag{10}$$

$$\frac{[X]_C^0 - [X]_C^\infty}{[X]_N^0 - [X]_N^\infty} = -\frac{V_N}{V_C} \tag{11}$$

$$\left(\alpha_N P_X + k_X^{N\to C}\right) = \frac{V_N}{\tau}\cdot\left(K_{eq}\frac{V_N}{V_C} + 1\right)^{-1} \tag{12}$$

In the following we shall show how to recover K_{eq}, τ, and the volume ratio V_N/V_C from a FRAP experiment. If one of the two volumes (typically V_N) is estimated from the fluorescence image of the cell, Eqs. 10, 11, and 12 allow for recovering of the two sums $\left(\alpha_C P_X + k_X^{C\to N}\right)$ and $\left(\alpha_N P_X + k_X^{N\to C}\right)$. In the absence of further information on the system it is not possible to work out separately the passive and active kinetic contributions for each compartment. We shall show, however, that much biochemical insight into the system under study can be acquired by means of a few reasonable assumptions.

Effect of binding on diffusion parameters

If X binds to other molecules in the cytoplasm or in the nucleoplasm, its permeability is expected to change. A significant example is the case of active transport, where binding to the importin complex drastically changes the translocation properties. Nonetheless, X may also bind to other intracellular components. For simplicity, we shall assume a general 1:1 binding scheme with the intracellular moiety Y

$$X + Y \underset{}{\overset{K_D}{\rightleftharpoons}} X\cdot Y$$

where K_D is the dissociation constant of the adduct. Note that X may interact with a number of biomolecular partners and thus K_D may have the meaning of an "average" dissociation constant. Additionally K_D can be different between the cytoplasm and the nucleoplasm, i.e., $(K_D)_C \neq (K_D)_N$, on account of the dissimilar physicochemical characteristics of the two compartments. The combination of the mass-action law and mass balance yields the global (or prebleach) concentration of X·Y complex

$$\xi_{C/N}\cdot [X]_{C/N}^0 = 0.5\left\{A - \left[A^2 - 4[X]_{C/N}^0\cdot[Y]_{C/N}^0\right]^{0.5}\right\} \tag{13a}$$

where

$$A = \left([\mathrm{X}]^0_{\mathrm{C/N}} + [\mathrm{Y}]^0_{\mathrm{C/N}} + (K_\mathrm{D})_{\mathrm{C/N}}\right) \tag{13b}$$

$\xi_{\mathrm{C/N}}$ is the molar fraction of bound X to Y, and subscript C/N indicates that the equation is valid for each compartment separately. It is worth noting that a further relation holds:

$$\xi_{\mathrm{C/N}} \cdot [\mathrm{X}]^0_{\mathrm{C/N}} = \theta_{\mathrm{C/N}} \cdot [\mathrm{Y}]^0_{\mathrm{C/N}} \tag{13c}$$

where $\theta_{\mathrm{C/N}}$ is the molar fraction of Y engaged in a complex with X. Equations 13a–c establish a link between FRAP-accessible parameters ($\xi_{\mathrm{C/N}}$) and the *global* concentration of the binding partners through the dissociation constant $(K_\mathrm{D})_{\mathrm{C/N}}$.

Let us now consider a fully general case where X binds to

- Importin receptor in the cytoplasm (global molar fraction of importin-bound X=χ_C)
- Cytoplasm components (global molar fraction of component-bound X=β_C)
- Exportin receptor in the nucleoplasm (molar fraction of exportin-bound X=χ_N)
- Nucleoplasm components (global molar fraction of component-bound X=β_N)

We shall also assume that the passive diffusion of bound X across the NE is negligible if compared to free X. This assumption is fully justified for importin–exportin complexes, whose N/C translocation is purely energy-dependent (i.e., active), and whenever binding takes place with immobile structures in one or both compartments; yet, this assumption is valid also when the bimolecular complex has a significantly larger size compared to X alone, a case that is frequently encountered in reality. Under this assumption we have

$$\alpha_{\mathrm{C/N}} \cdot P_\mathrm{X} = \left(1 - \chi_{\mathrm{C/N}} - \beta_{\mathrm{C/N}}\right) P_\mathrm{X} \tag{14}$$

and the scaling factor $\alpha_{\mathrm{C/N}}$ assumes the meaning of global molar fraction of free X in the cytoplasm or in the nucleoplasm.

Now, let us now introduce the two parameters $\Phi_{\mathrm{C}\to\mathrm{N}}$ and $\Phi_{\mathrm{N}\to\mathrm{C}}$ defined as

$$\Phi_{\mathrm{C}\to\mathrm{N}} = \left(\alpha_\mathrm{N} P_\mathrm{X} + k_\mathrm{X}^{\mathrm{N}\to\mathrm{C}}\right)\left(K_\mathrm{eq} - 1\right)[\mathrm{X}]^0_\mathrm{C} \tag{15a}$$

$$\Phi_{\mathrm{N}\to\mathrm{C}} = \left(\alpha_\mathrm{C} P_\mathrm{X} + k_\mathrm{X}^{\mathrm{C}\to\mathrm{N}}\right)\left(K_\mathrm{eq}^{-1} - 1\right)[\mathrm{X}]^0_\mathrm{N} \tag{15b}$$

$\Phi_{\mathrm{C}\to\mathrm{N}}$ and $\Phi_{\mathrm{N}\to\mathrm{C}}$ will be hereafter denoted as excess fluxes of X (the first toward the nucleus, the second toward the cytoplasm). Both parameters can be computed from quantities available after a FRAP analysis (Eqs. 10, 11, and 12).

Substituting Eqs. 8, 10, 14, in 15a, b yields

$$\Phi_{\mathrm{C}\to\mathrm{N}} = [\chi_\mathrm{C} \cdot (\nu_{\mathrm{C}\to\mathrm{N}} - P_\mathrm{X}) - \chi_\mathrm{N} \cdot (\nu_{\mathrm{N}\to\mathrm{C}} - P_\mathrm{X}) + P_\mathrm{X} \cdot (\beta_\mathrm{N} - \beta_\mathrm{C})][\mathrm{X}]^0_\mathrm{C} \tag{16a}$$

$$\Phi_{\mathrm{N}\to\mathrm{C}} = [\chi_\mathrm{N} \cdot (\nu_{\mathrm{N}\to\mathrm{C}} - P_\mathrm{X}) - \chi_\mathrm{C} \cdot (\nu_{\mathrm{C}\to\mathrm{N}} - P_\mathrm{X}) + P_\mathrm{X} \cdot (\beta_\mathrm{C} - \beta_\mathrm{N})][\mathrm{X}]^0_\mathrm{N} \tag{16b}$$

Equations 16a, b are the fundamental relations of our model: plots of $\Phi_{\mathrm{C}\to\mathrm{N}}$ vs. $[\mathrm{X}]^0_\mathrm{C}$ and of $\Phi_{\mathrm{N}\to\mathrm{C}}$ vs. $[\mathrm{X}]^0_\mathrm{N}$ contain all the binding and dynamic information relevant to the NE translocation process. The following significant example (active import/passive diffusion) will explain this in more detail.

Active import/passive diffusion

We shall assume that

- X is actively imported in the nucleus by importin Y.
- Passive diffusion of X across the NE is allowed.
- Binding to other moieties is negligible compared to importin.

These conditions are translated into $\chi_\mathrm{N} = 0; \beta_{\mathrm{C/N}} \approx 0$, and therefore, from Eqs. 14, 15a, and 16a

$$\Phi_{\mathrm{C}\to\mathrm{N}} = P_\mathrm{X}\left(K_\mathrm{eq} - 1\right)[\mathrm{X}]^0_\mathrm{C} \tag{17a}$$

$$\Phi_{\mathrm{C}\to\mathrm{N}} = (\nu_{\mathrm{C}\to\mathrm{N}} - P_\mathrm{X})\chi_\mathrm{C} \cdot [\mathrm{X}]^0_\mathrm{C} \tag{17b}$$

In this context, $\Phi_{\mathrm{C}\to\mathrm{N}}$ corresponds to the difference between the global C→N flux (passive+active) and the theoretical pure passive C→N flux of all X: we shall name it *excess active flux* of X. We remind that Eq. 17a provides the way to compute $\Phi_{\mathrm{C}\to\mathrm{N}}$ from FRAP quantities (Eqs. 10, 11, and 12).

Now, by combining Eqs. 13a with 17b (here $\xi_\mathrm{C} = \chi_\mathrm{C}$), we have

$$\Phi_{\mathrm{C}\to\mathrm{N}} = (\nu_{\mathrm{C}\to\mathrm{N}} - P_\mathrm{X})0.5\left\{A - \left[A^2 - 4 \cdot [\mathrm{X}]^0_\mathrm{C} \cdot [\mathrm{Y}]^0_\mathrm{C}\right]^{0.5}\right\} \tag{18}$$

with A expressed by Eq. 13b. If we assume that the cytoplasmic concentration of importin Y ($[\mathrm{Y}]^0_\mathrm{C}$) is approximately constant in all cells (Y is a structural biological factor), while the cell expression of actively imported cargo X can vary (see examples in the next sections), then—according to Eq. 18—$\Phi_{\mathrm{C}\to\mathrm{N}}$ is expected to grow linearly with $[\mathrm{X}]^0_\mathrm{C}$ until a significant fraction of X is engaged in the complex with the importin transporter, then it must level off owing to importin

saturation. Thus an experimental plot of $\Phi_{C\to N}$ vs. $[X]_C^0$ will allow for determination of $(K_D)_C$ by fitting to Eqs. 18 and 13b.

Furthermore, let us rewrite Eq. 17b by means of 13c

$$\Phi_{C\to N} = \theta_C \cdot [Y]_C^0 \cdot (\nu_{C\to N} - P_X) \tag{19}$$

If active transport is much more efficient than passive translocation, a case usually found in practice (see next section), we can assume $\nu_{C\to N} \gg P_x$, and therefore

$$\Phi_{C\to N} \cong \theta_C \cdot V_{C\to N}, \tag{20}$$

where the product $[Y]_C^0 \cdot \nu_{C\to N}$ is recast into the parameter $V_{C\to N}$. At importin saturation ($\theta_C \to 1$), $V_{C\to N}$ expresses the translocation efficiency, in terms of imported molecule per second, of the importin complex through the NPC (i.e., $\nu_{C\to N} \cdot [Y]_C^0$). Assuming that all complexes of importin with NLS moieties share the same translocation rate (in keeping with the active transport mechanism described earlier), $V_{C\to N}$ represents *the intrinsic dynamic parameter of nuclear import*. $V_{C\to N}$ is calculated as the asymptote of the $\Phi_{C\to N}$ vs. $[X]_C^0$ curve by fitting to Eqs. 18 and 13b.

It is worth mentioning that the above analysis can be applied to nuclear export by considering complex formation in the nucleus, and rearranging Eqs. 16b and 17b similarly to what was done for Eqs. 16a and 17a.

Experimental procedures

Materials preparation

Details of the preparation of protein plasmids and their expression in cells can be found in elsewhere [22]

Fluorescence microscopy and image analysis

Cell fluorescence was measured using a Leica TCS SP2 or TCS SP5 inverted confocal microscope (Leica Microsystems AG, Wetzlar, Germany) interfaced with an Ar laser for excitation at 458, 476, 488, and 514 nm, and with a helium–neon laser for excitation at 561 and 633 nm. Glass-bottomed Petri dishes containing transfected cells were mounted in a thermostated chamber (Leica Microsystems) and viewed with a 40× 1.25 numerical aperture oil immersion objective (Leica Microsystems). Live cell imaging was always performed at 37 °C with 5 % CO_2. The images were collected using 10–20-μW excitation power at the sample and monitoring the emission by means of the AOBS-based built-in detectors of the confocal microscope. The following collection ranges were adopted: 500–550 nm (EGFP) and 580–650 nm (mCherry). Background signal was subtracted in all images. Data were analyzed using a code specifically written for the Igor Pro software package (Wavemetrics, Lake Oswego, USA).

FRAP measurements and data recovery

In order to measure nucleocytoplasmic translocation, our FRAP experiment protocol starts with an image of the cell (prebleach image) followed by bleaching of the nucleus or the cytoplasm (excitation wavelength for EGFP bleaching 488 nm; excitation wavelength for mCherry bleaching 561 nm) and then by a time-lapse acquisition of the cell fluorescence. Nuclear bleaching is accomplished by a single-point bleach (non-scanning mode) near the center of the nucleus; cytoplasmic bleaching is obtained by performing repeated scans of the whole cytoplasmic region. In both cases, the laser is set at full power (150 μW, corresponding to 300–400 kW/cm^2) for the minimum time required to photobleach most of the compartment fluorescence (4–10 s). Acquisition of fluorescence recovery starts within a few milliseconds after the end of bleaching, with sampling rate tuned to the NE crossing rate of the cargo under test (from one image every 6 s for fast shuttling to one image every 30 s for slow shuttling). Pinhole size is set to the optimal value of 1.0 airy to provide confocality to cell imaging.

Concerning FRAP data analysis, a direct proportionality between cargo concentration [X] and its fluorescence can be assumed. Thus Eqs. 9a, b and 11 can be rewritten as

$$F_C(t) = F_C^\infty + \left(F_C^0 - F_C^\infty\right) \cdot \exp(-t/\tau) \tag{21a}$$

$$F_N(t) = F_N^\infty + \left(F_N^0 - F_N^\infty\right) \cdot \exp(-t/\tau) \tag{21b}$$

$$\frac{F_C^0 - F_C^\infty}{F_N^0 - F_N^\infty} = -\frac{V_N}{V_C} \tag{22}$$

and $K_{eq} = F_N^\infty / F_C^\infty$. The parameter K_{eq}^{pre} is also computed as the ratio of nuclear and cytoplasmic fluorescence *before* bleaching. A difference between K_{eq} and K_{eq}^{pre} indicates the presence of a so-called *immobile fraction*, i.e., a fraction of cargo irreversibly bound to biomolecular components. In such a case, only K_{eq} is used for the analysis.

The recovery data for both compartments are fitted to Eq. 21a, b and yield K_{eq}. The volume ratio is obtained through Eq. 22. Note that before fitting experimental fluorescence values, these must be normalized by the fluorescence of the entire cell at the same time, in order to minimize the impact of cell motility and defocusing on recovery curves and to correct for bleaching caused by imaging.

Determination of nuclear volume

V_N is estimated by assuming an ellipsoid shape for the nucleus with semi-axes d_x, d_y, and d_z by the equation $V_N = (4\pi/3) \cdot d_x \cdot d_y \cdot d_z$. The three axes can be determined from confocal images of the nucleus, and in most cases we set d_z equal to d_y, the smallest semi-axis in the horizontal plane. Indeed, the latter approach is justified by the similarity of the two semi-axis in most cells (maximum deviation 10 %). It is worth noting that relative uncertainties in the V_N value reflect linearly in uncertainties in all primary dynamic parameters that are relevant to our analysis (i.e., P_X,$k_X^{C\to N}$, $k_X^{N\to C}$), as can easily be inferred by inspection of Eq. 12.

Determination of intracellular concentrations

Intracellular concentration of EGFP can be calculated by a calibration method that makes use of a fluorescein–glycine adduct as a fluorescent standard, according to a recently published procedure [24].

FRAP analysis of nucleocytoplasmic exchange

In this section, we demonstrate by paradigmatic examples the ability of our approach to interpret FRAP data of nucleocytoplasmic translocation. First, we test our model on passive diffusion alone, checking whether it fully accounts for the observable phenomenology in vivo. Then, we apply our model to a mixed passive-active transport system operating in the cell. Such a system is representative of a broad class of relevant transport processes occurring in live cells.

Benchmark of passive nucleocytoplasmic diffusion: determination of nuclear pore radius

We studied by FRAP the passive nucleocytoplasmic diffusion of F64L/S65T GFP (EGFP) in CHO cells. EGFP is a green-enhanced variant of GFP that retains all the structural properties of the parent protein. Like GFP, EGFP has a molecular weight of 27 kDa that allows for efficient passive diffusion through the NPC (Scheme 1, A.1).

Similarly, EGFP does not exhibit any nuclear localization or export signal, and one can further assume that cytoplasmic and nucleoplasmic sides of the NE possess the same permeability to EGFP, on account of the almost null interactions of GFPs with the cellular environment. In our model, these conditions are expressed by

$$\chi_{C/N} = 0, \beta_{C/N} = 0, K_{eq} = 1 \qquad (22)$$

A virtually equimolar distribution of EGFP between the nucleus and the cytoplasm was always observed before

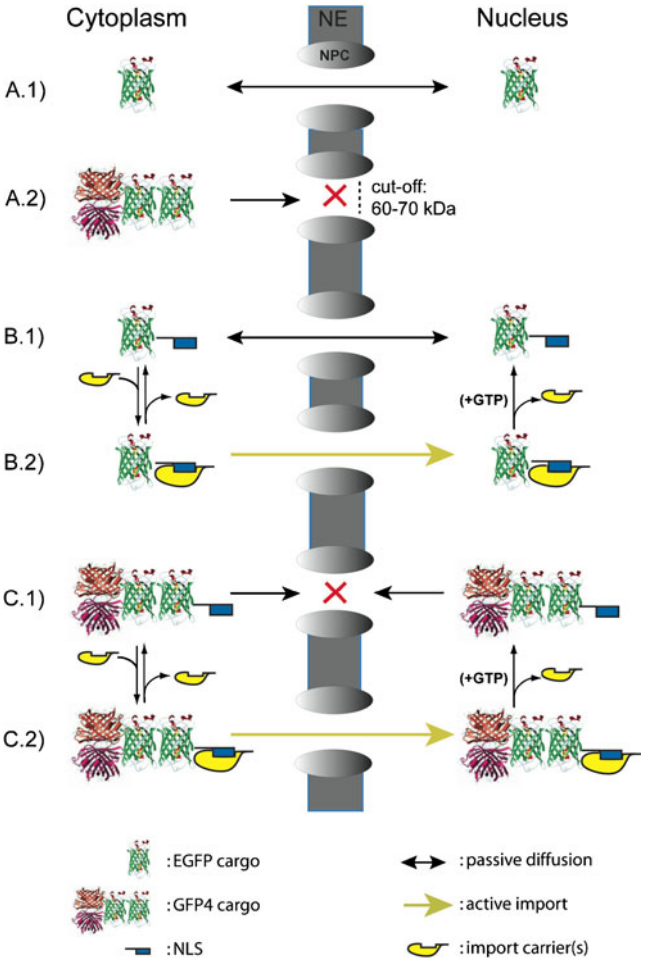

Scheme 1 The single EGFP cargo (27 kDa) can freely diffuse between nucleus and cytoplasm (**A.1**), whereas the GFP_4 cargo is too large (110 kDa) to cross the NE (**A.2**) (the cutoff size for passive diffusion through the pore is around 60–70 kDa). The NLS-tagged EGFP cargo can either shuttle across the NE with its proper diffusion characteristics (**B.1**) or bind to import carriers in the cytoplasm (**B.2**). In the latter case, it is imported into the nucleus where it dissociates from the carrier by an energy-consuming process. Once free in the nucleus it can diffuse back to cytoplasm (as shown in **B.1**). Conversely, the NLS-tagged GFP_4 cargo can not diffuse across the NE (**C.1**). It can only bind to import carriers in the cytoplasm, cross the NE, and dissociate once in the nucleus (**C.2**). This overall irreversible process (**C.1**, **C.2**) leads to the accumulation of NLS-GFP_4 in the nucleus

bleaching and after recovery (deviations, if present, are within 10 %; Fig. 1a, left). Bleaching of the nucleus led to fluorescence recovery in this compartment at the expense of cytoplasmic fluorescence (Fig. 1a, b). The opposite trend was observed upon cytoplasm bleaching (Fig. 1b). In both cases FRAP curves were well described by monoexponentials with $\tau \cong 60$ s (Fig. 1b). Remarkably, we found no correlation between P_{EGFP} and cellular concentration of EGFP in a broad range (10 nM to 260 μM, N=22 cells; Fig. 1c). Hence, diffusion of a medium-sized biochemically inert cargo through the pore is unaffected by the number of cargo

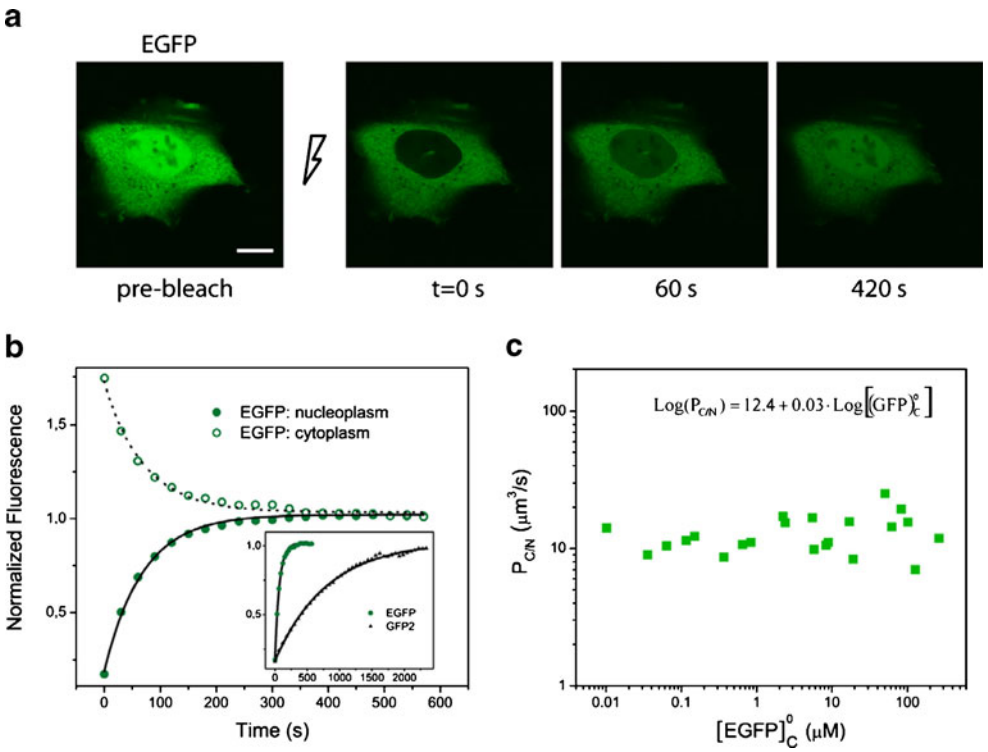

Fig. 1 In vivo analysis of reversible passive diffusion. **a** Prebleach image of the cell was collected by confocal laser scanning microscopy; *scale bar* 10 μm. Photobleaching was accomplished by irradiating a single point in the nucleus with high laser power (150 μW, excitation wavelength 488 nm) for 4–10 s. Fluorescence recovery was recorded (excitation wavelength 488 nm, emission wavelength interval 500–550 nm) at different times; selected images are reproduced with the time of acquisition. **b** Time course of nucleoplasmic fluorescence recovery (*filled green circles*) for the cell shown in **a**. Cytoplasmic fluorescence concomitantly decreases as EGFP diffuses from cytoplasm to nucleus (*open green circles*). This symmetric process shows the same kinetics, yielding a time constant (τ) of approximately 60 s (single-exponential fits are represented by *solid black lines*). The *inset* highlights the difference in recovery kinetics between EGFP and GFP_2 cargoes. **c** The permeation coefficient (P_{EGFP}) derived by FRAP analysis is here plotted cell-by-cell against the corresponding EGFP cytoplasmic concentration; the lack of correlation between these parameters indicates that diffusion of the EGFP cargo through the pore is not affected by the number of molecules in a wide concentration range (from 10 nM to 260 μM)

molecules in a concentration range much larger than the physiologically relevant one. This finding is perfectly consistent with a diffusion mechanism driven solely by the concentration gradient between the two compartments and it indicates that no cargo crowding at the NPC is changing this biophysical pattern.

Next, we considered a double-size GFP cargo (GFP_2) obtained by the molecular fusion of EBFP (a blue mutant of GFP [25]) and EGFP via a 17 amino acid-long flexible linker. The molecular weight of GFP_2 (56 kDa) is close to the estimated molecular cutoff size for passive diffusion through the NPC (60–70 kDa).

Accordingly, we found that nucleocytoplasmic trafficking of GFP_2 was significantly hampered if compared to EGFP (τ=1,178±292 s, N=8 cells; Fig. 1b, inset), and P_{GFP2}=1.1±0.5 μm³/s. Applying Eq. 7 to both EGFP and GFP_2 and taking the ratio between the left and right sides we have

$$\frac{P_{EGFP}}{P_{GFP_2}} \cdot \frac{D_{GFP_2}}{D_{EGFP}} = \frac{f\left(r_{EGFP}, r_p\right)}{f\left(r_{GFP_2}, r_p\right)} \tag{23}$$

where f is the polynomial function described in [23]. We recently reported that D_{EGFP}=20±5 μm²/s and D_{GFP2}=13.5±5.5 μm²/s [22], in good agreement with previously published results [26, 27]. The hydrodynamic radius of EGFP was determined to be 2.82 nm [28]. The radius of GFP_2 can be obtained by the Stokes–Einstein relationship starting from its cytoplasmatic diffusion coefficient and using EGFP as reference. We find r_{GFP_2} = 4.09nm, a value in good agreement to that structurally determined by SAXS for similar EBFP–EGFP tandem constructs [29]. Inserting these data in Eq. 23 we obtain r_p=5.33 nm. This result is in excellent agreement with a previous measurement of the mean pore radius (5.35 nm [15]) and validates our FRAP analysis. A procedure to calculate r_p analogous to that presented here was also reported by Chen et al. [27]. Interestingly, Mohr et al. calculated a much narrower size of pore, r_p=2.66 nm, although these authors used a simplified form of polynomial function f in Eq. 2 and permeabilized cells [30]; nonetheless, the same authors reported that a minor fraction of NPC did allow for the passive diffusion of larger cargoes.

Benchmark of mixed active-passive transport: SV40 NLS-linked cargoes

The 11 amino acid SV40 NLS is a powerful promoter of active transport from the cytoplasm towards the nucleus. It is well known that the NLS motif binds to importin-α (Imp-α) in the cytoplasm and promotes the formation of an NLS: importin-α:importin-β complex [31]. This complex is subsequently relocated into the nucleus through facilitated transport across the NPC. The complex is disassembled in the nucleus by the action of RanGTP [19] (whose nuclear accumulation is a function of metabolic energy), and the NLS-linked molecule is released. The active transport capability of NLS is clearly demonstrated when it is bound to a cargo which is otherwise unable to cross the nuclear barrier by passive diffusion owing to its large size. A GFP tetramer (GFP_4, 110 kDa) is a good example of such a cargo: by itself it is found only in the cytoplasm (Scheme 1, A.2 and Fig. 2a, left), but its NLS-fusion protein relocates completely into the nucleoplasm from where it can not escape by passive diffusion owing to its size (Scheme 1, C.1–2 and Fig. 2a, right).

The smaller construct NLS-EGFP represents an excellent model to study active import in the presence of passive diffusion by FRAP. Indeed, NLS-EGFP has virtually the same molecular weight as EGFP (28 kDa vs. 27 kDa), which allows efficient passive diffusion through the NPC concomitantly with active import into the nucleus (Scheme 1, B.1–2).

The resulting phenotype shows preferential fluorescence localization in the nucleus, but some residual fluorescence is also detectable in the cytoplasm (Fig. 2b, left). The concurring action of passive diffusion is also demonstrated by the effect of energy depletion. In fact, when cells expressing NLS-EGFP are subjected to an energy-depletion treatment, active import to the nucleus is no longer possible and a homogeneous intracellular distribution of fluorescence is observed (Fig. 2b, right). The latter phenotype stems from pure passive nucleocytoplasmic diffusion, as already discussed for the case of EGFP alone. The presence of a significant passive diffusion component in NLS-EGFP nucleocytoplasmic shuttling was confirmed by the comparison between the nuclear FRAP curves of NLS-EGFP and NLS-GFP_2 (Fig. 2c): as expected fluorescence recovery of the latter protein is significantly slower, on account of the much lower permeability of the NE to the GFP_2 construct.

NLS-EGFP shows the recovery behavior of EGFP at both cytoplasm and nucleoplasm levels (Fig. 2c, inset). Recovery curves are well fitted to monoexponentials, yielding a τ value ranging from 40 to 300 s, with a marked dependence on protein expression level as expected for a different concentration of bound NLS: Imp-α complexes. Since the nucleocytoplasmic transport behavior of EGFP matches those of the "Active import/passive diffusion" case described earlier, we set out to analyze FRAP data with the help of Eqs. 17a, 18, 19, and 20 and determination of $[\mathrm{NLS}-\mathrm{EGFP}]_C^0$ by our calibration method [24].

Figure 2d shows the plot of $\Phi_{C\to N}$ vs. $[\mathrm{NLS}-\mathrm{EGFP}]_C^0$ for the experiments that we carried out in living CHO cells [24]. It is worth noting that $[\mathrm{NLS}-\mathrm{EGFP}]_C^0$ (and its related function $\Phi_{C\to N}$) spans a broad concentration interval owing to the large expression variability of the NLS-EGFP cargo. $\Phi_{C\to N}$ increases linearly up to $[\mathrm{NLS}-\mathrm{EGFP}]_C^0$= 15–20 μM and then levels off. This trend suggests that 15–20 μM is the threshold concentration at which the endogeneous Imp-α/Imp-β transport complex starts operating at its maximum efficiency.

Plot of $\Phi_{C\to N}$ vs. $[\mathrm{NLS}-\mathrm{EGFP}]_C^0$ allows for the calculation of $V_{C\to N}$ and $(K_D)_C$ by fitting to Eqs. 18 and 13b with X=NLS-EGFP and Y=Imp-α (Fig. 2d, black line). In all calculations we set $[\mathrm{Imp}-\alpha]_C^0$ = 1 μM, which is the reported physiological concentration of Imp-α in a living cell [32]. The fitting procedure yielded $V_{C\to N}$ = 177,000±14,500 molecule/s (corresponding to $\nu_{C\to N}$=290 $\mu m^3/s$) and $(K_D)_C$ = 16±7 μM [24]. Assuming 2×10^3 NPCs per nucleus [17], this value translates into about 90 molecule/s per single NPC (Table 1), i.e., an intrinsic translocation time of importin complex around 11 ms. Remarkably, the latter value is in excellent agreement with single-molecule correlation measurements performed on NLS-GFP either on an ensemble of pores [33] or at the single-pore level [34]. These data are also consistent with the C→N flux of the import complex calculated at physiological importin concentration by Ribbeck and Gorlich [17]. As expected, the active translocation rate does not depend on the size of cargo, as verified for NLS-$EGFP_2$ by analogous FRAP experiments [24]. Additionally, the $\Phi_{C\to N}$ vs. $[\mathrm{NLS}-\mathrm{EGFP}]_C^0$ plot in CHO was found to be almost the same in different cell lines such as HeLa and U2OS, thus highlighting the remarkable generality of the calculated $V_{C\to N}$ and $(K_D)_C$ [24]. This would suggest highly conserved features of the import machinery in eukaryotes.

Earlier reports show in vitro $(K_D)_C$ values in the 10–100 nM range [20], indicating much higher affinity between NLS and importin-α in vitro than found at the intracellular level. The complex biological nature of the cytoplasm accounts well for the observed discrepancy. In the cytoplasm, in fact, there can be other NLSs that compete for Imp-α, other moieties that bind to the NLS, and a non-uniform distribution of the Imp-α/Imp-β active complex [24].

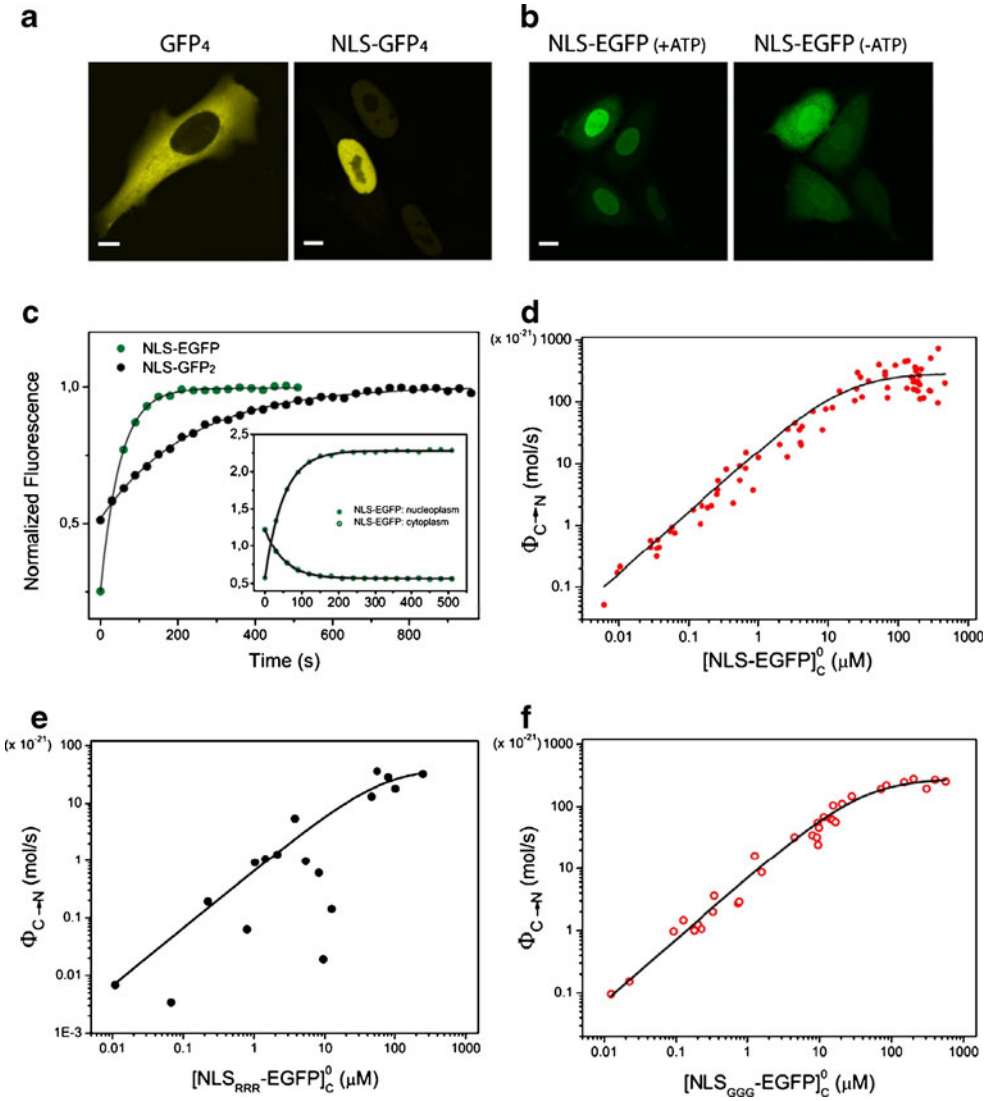

Fig. 2 In vivo analysis of active import. **a** As expected from its molecular weight (110 kDa), the untagged GFP_4 cargo is excluded from the nucleus, as it is not able to diffuse through the pore (*left panel*). Conversely, NLS-tagged GFP_4 is almost exclusively localized in the nucleus (*right panel*), as it imported by specific carriers while its nucleus-to-cytoplasm diffusion is impaired by cargo size. **b** The NLS of SV40 is able to accumulate the EGFP cargo into the nucleus under physiological conditions (+ATP, *left panel*). This process depends on metabolic energy: accordingly, after 15 min of energy depletion treatment, NLS-EGFP equilibrated between nucleus and cytoplasm. *Scale bars* 10 μm. **c** Time course of nucleoplasmic fluorescence recovery (*filled green circles*) after nuclear photobleaching of NLS-EGFP compared to $NLS\text{-}GFP_2$ (*black filled circles*). *Inset* cytoplasmic (*open green circles*) and nuclear (*filled green circles*) fluorescence curves after NLS-EGFP nuclear photobleaching. Monoexponential fitting yields a time constant (τ) of approximately 60 s (single-exponential fits are represented by *solid black lines*). **d**, **f** Plots of $\Phi_{C\to N}$ vs. the global cytoplasmic concentration of NLS-EGFP (*full red circles*, **d**) or NLS_{RRR}-EGFP (*full black circles*, **e**) or NLS_{GGG}-EGFP (*empty red circles*, **f**); fitting curves to Eqs. 18 and 13b are reported in all plots as *black lines*

Modulation of translocation activity of SV40 NLS and comparison with Tat[11] peptide

The 48–58 stretch YGRKKRRQRRR of HIV transactivator protein Tat[11] is a positively charged peptide that displays chemical features similar to SV40 NLS. Previous studies showed that Tat[11] is composed of two functional domains: the first 8 amino acids promoting active nuclear import, and the latter three arginines which bind cell-wide to anionic species such as RNA [21, 35]. The strong binding characteristics of RRR can suppress active nuclear transport and Tat[11] was shown to evenly distribute between cytoplasm and nucleus [22]. In order to test the effect of competitive binding on the nuclear import of NLS-EGFP, the EDP terminal sequence of NLS was replaced by RRR (NLS_{RRR}-EGFP) and FRAP experiments were carried out. Consistently with Tat[11], the resulting almost even nucleocytoplasmic distribution reflected the reduced import

capability of NLS_{RRR}-EGFP. From the fit of $\Phi_{C\to N}$ vs. [NLS_{RRR}-GFP] to Eqs. 18 and 13b, we found $V_{C\to N}$ = 13±3 molecules/s per single NPC and $(K_D)_C$ = 65±41 μM (Fig. 2e, Table 1). Thus, the short RRR stretch decreases fourfold the binding affinity of NLS towards Imp-α and sevenfold the translocation efficiency of the NLS–Imp-α complex. Additionally, the P_x value of NLS_{RRR}-EGFP is 2.0 ±0.8 $\mu m^3/s$, about 2.5 times smaller than that of NLS-GFP (5.2±2 $\mu m^3/s$). We attribute these effects to RRR-induced affinity towards polyanionic moieties, which compete with importin complexation and greatly enhance the size of the diffusing moiety.

Interestingly, replacement of the RRR terminal sequence with GGG, a non-charged, flexible domain, successfully removes this hampering of nuclear import. In particular, fitting of the $\Phi_{C\to N}$ vs. [NLS_{GGG}-EGFP] plot (Fig. 2f) leads to $V_{C\to N}$ = 87±4 molecules/s per single NPC and $(K_D)_C$ = 38±5 μM (Table 1). These findings show that the GGG domain is capable to fully restore the active import process (as reflected by the same $V_{C\to N}$ values for NLS-EGFP and NLS_{GGG}-EGFP) although some binding affinity is lost ($(K_D)_C$ is about twofold as large). Yet, the NE passive permeability of NLS_{GGG}-EGFP is almost the same as NLS (5.8±2.8 $\mu m^3/s$ vs. 5.2±2 $\mu m^3/s$), strongly suggesting that the two NLS species have the same size (Table 1). This in turn excludes a contribution of binding competitors to the observed lower affinity of NLS_{GGG}-EGFP towards Imp-α. Taken together these results clearly indicate that importin binding and transport are two independent processes that can be separately modulated.

Limits of validity of the "well-stirred compartment" assumption

Our FRAP analysis of nucleocytoplasmic transport is based on the assumption that diffusion within each compartment is much faster than translocation across the NE ("well-stirred compartment" assumption). We now discuss the limits of this assumption in relation to the FRAP studies reported in this article.

Unless some special forms of transport is active (e.g., transport along some cytoskeletal component), the intracompartment diffusion of a given molecule can be described by a simple 3D random walk, i.e.,

$$\tau_i = \frac{w^2}{4D} \tag{24}$$

where τ_i is the characteristic time associated with diffusion between two points separated by a distance w. In order to demonstrate that nucleus and cytoplasm are two well-stirred compartments in which internal diffusion takes place on a much shorter timescale with respect to translocation across the NE, one must compare τ_i with τ experimentally obtained by Eq. 21a, b and show that $\tau \gg \tau_i$. In the following we shall assume w=10 μm as characteristic distance between a generic cytoplasm point and the NE and consider the well-stirred assumption valid when $\tau_i/\tau < 0.1$. Our goal here is to identify the minimum cargo size (i.e. ,the hydrodynamic radius) for which this condition holds.

For our calculation, we can use EGFP as a benchmark. The bulk intracellular diffusion coefficient of a cargo molecule X can be recovered by applying the Stokes–Einstein relation to both X and EGFP. We have

$$D_X = D_{EGFP} \cdot \frac{r_{EGFP}}{r_X} \tag{25}$$

where $D_{EGFP} \approx 20\ \mu m^2/s$ and r_{EGFP}=2.82 nm. Once D_X is known we can apply Eq. 7 to both X and EGFP and take the ratio of each side, obtaining the permeability coefficient P_X as

$$P_X = P_{EGFP} \cdot \frac{f(r_X, r_p) \cdot D_X}{f(r_{EGFP}, r_p) \cdot D_{EGFP}} \tag{26}$$

For the sake of generality, we shall suppose that X can undergo both passive diffusion and nuclear active import. Figure 3 shows the plot of the τ_i/τ ratio against r_X (in nm), as calculated by the described approach, assuming V_C= 4,000 μm^3 and V_N=1,000 μm^3. Note that the ratio is calculated for the two limit cases χ_C=0 (only passive diffusion, red curve), χ_C=1 (only active transport from cytoplasm to nucleus, blue curve). For the latter case, according to our experimental results we took $\nu_{C\to N}$=290 $\mu m^3/s$. Intermediate cases must fall between these two curves.

Analysis of the passive diffusion curve reveals that $\tau_i/\tau < 0.1$ for r_X>1.78 nm. Hence, the well-stirred compartment assumption is well justified for our FRAP analysis of EGFP (r=2.82 nm) and GFP_2 (r=4.09 nm) data. Actually, $r_X \approx$ 1.78 nm corresponds to cargoes around 10 kDa; we can conclude that nucleocytoplasmic passive diffusion of cargoes larger than 10 kDa is amenable to our FRAP model because intracompartment and nucleocytoplasmic diffusion dynamics are well decoupled.

Conversely, the pure active-import curve never shows $\tau_i/\tau < 0.1$. Nonetheless, our findings clearly demonstrate that

Table 1 Thermodynamic and dynamic parameters for NLS-EGFP mutants

Protein	$(K_D)_C$ (μM)	$V_{C\to N}$ (molecules/s·NPC)	P_x ($\mu m^3/s$)
NLS-EGFP	16±7	90±7	5.8±2.8
NLS_{RRR}-EGFP	65±41	13±3	2.0±0.8
NLS_{GGG}-EGFP	38±5	87±4	5.2±2.0

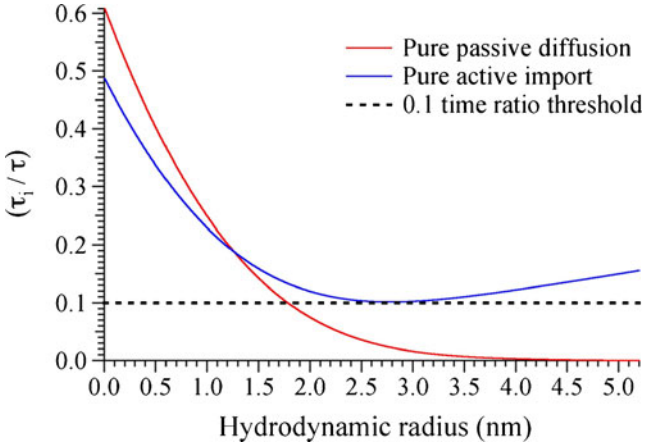

Fig. 3 Ratio of characteristic times of intracompartment diffusion and nucleocytoplasmic translocation plotted against the hydrodynamic radius of cargo. *Red line* ratio calculated for pure passive diffusion between nucleus and cytoplasm, i.e., $\chi_{C/N}=0$, where $\chi_{C/N}$ represents the molecular fraction of cargo engaged in a complex with intracellular importins or exportins. *Blue line* ratio calculated for a cargo whose transport from cytoplasm to nucleoplasm is governed only by interaction with the importin complex; however, the same cargo can be recycled from nucleoplasm to cytoplasm by means of size-dependent passive diffusion. *Dotted line* represents the ratio value of 0.1 for which we may assume poor coupling between the intracompartment and nucleocytoplasmic diffusional processes

full binding to importin ($\chi_C=1$) is very unlikely at physiological cargo and importin concentrations, given the rather high value of the in vivo dissociation constant between these two species (Table 1). Consistently, for NLS-EGFP the minimum τ of nucleocytoplasmic transport was 40 s, a value much larger of the 1–2 s that we can estimate for τ_i. This difference would clearly increase for larger cargoes such as those usually engaged in active transport. Hence, the well-stirred compartment assumption is fully applicable in the presence of active nuclear import at physiological concentrations.[1]

It is worth noting that the peculiar convex form of the purely active-import ratio curve stems from the counterbalancing effect of K_{eq} and P_X: for a *small molecule*, P_X is obviously high, but K_{eq} is low because in this case C→N transfer is driven only by active transport (here $\nu_{C\to N} \ll P_X$); conversely, for a large molecule P_X can be very low but now K_{eq} is very high ($\nu_{C\to N} \gg P_X$, remember also the GFP_4 phenotype; Fig. 2a, right).

Conclusions

Fluorescence recovery after photobleaching stands out as one of the most powerful techniques available to get insight into the intracellular environment. Several reasons justify its success in biophysics and molecular biology: (1) FRAP is a relaxation technique, i.e., it focuses on molecular changes rather than on absolute properties; (2) FRAP entails just the change of optical properties of the probe connected to the biomolecule of interest, and almost never affects the biochemistry of the latter; (3) FRAP focuses on molecular diffusion, which is connected to virtually all biochemical processes; (4) the discovery and engineering of autofluorescent proteins gave FRAP the ideal probe to work with, owing to the genetic encoding of FP's fluorescence.

In this work we showed how FRAP can be useful to understand the molecular mechanisms at the basis of nucleocytoplasmic transport. Indeed, diffusion between two or more compartments separated by a membrane is amenable to a rather simple mathematical treatment. We reported here a general model of translocation across the nuclear envelope entailing also binding reactions and we showed which parameters can be recovered by FRAP. Our analysis demonstrates that molecular crowding at the nuclear pore does not hamper passive diffusion. On the basis of an established model of membrane permeability, and using GFPs as benchmarks, we were able to estimate nuclear pore size. We also tackled the issue of active nuclear import by using the monopartite NLS motif of simian virus 40 (SV40) linked to several GFP-based constructs. Our FRAP data yielded values for the maximum rate of active transport to the nucleus and the binding affinity between an NLS sequence and its transporter protein importin-α. Furthermore, by means of rational mutagenesis, we investigated the role of the 3 amino acid terminal stretch of NLS to modulate active nuclear transport characteristics. In particular, replacement of the parent EDP stretch with RRR hampers active transport by establishing strong electrostatic interactions with polyanionic biomolecules (e.g., RNA). When EDP is replaced by the non-charged and flexible GGG motif, the affinity of NLS towards importin decreases, but no changes in the translocation rate are observed, supporting our view of independent binding and transport processes.

These data provide a fully quantitative description of the nucleocytoplasmic translocation and will be useful in engineering new peptide sequences for selected nuclear targeting.

Acknowledgements We thank Dr. Matilde Marchi and Dr. GianMichele Ratto for stimulating discussions. This work was partially supported by the Italian Ministry for University and Research (MiUR) under the framework of the FIRB project RBLA03ER38 and by Fondazione Monte dei Paschi di Siena.

[1] Note that for NLS-EGFP this assumption is also valid at non-physiological very high cargo concentrations, as in that situation a large fraction of nucleocytoplasmic transport is accounted for by passive diffusion.

References

1. Lippincott-Schwartz J, Altan-Bonnet N, Patterson GH (2003) Nat Cell Biol 5(Suppl):S7–14
2. Peters R, Peters J, Tews KH, Bahr W (1974) Biochim Biophys Acta 367:282–294
3. Lippincott-Schwartz J, Snapp E, Kenworthy A (2001) Nat Rev Mol Cell Biol 2:444–456
4. Phair RD, Misteli T (2000) Nature 404:604–609
5. Dorsch S, Klotz KN, Engelhardt S, Lohse MJ, Bunemann M (2009) Nat Methods 6:225–230
6. van Royen ME, Farla P, Mattern KA, Geverts B, Trapman J, Houtsmuller AB (2009) Methods Mol Biol 464:363–385
7. Wehrle-Haller B (2007) Methods Mol Biol 370:173–202
8. Costa M, Marchi M, Cardarelli F, Roy A, Beltram F, Maffei L, Ratto GM (2006) J Cell Sci 119:4952–4963
9. Braeckmans K, Peeters L, Sanders NN, De Smedt SC, Demeester J (2003) Biophys J 85:2240–2252
10. Jovanovic-Talisman T, Tetenbaum-Novatt J, McKenney AS, Zilman A, Peters R, Rout MP, Chait BT (2009) Nature 457:1023–1027
11. Alber F, Dokudovskaya S, Veenhoff LM, Zhang W, Kipper J, Devos D, Suprapto A, Karni-Schmidt O, Williams R, Chait BT, Sali A, Rout MP (2007) Nature 450:695–701
12. Patel SS, Belmont BJ, Sante JM, Rexach MF (2007) Cell 129:83–96
13. Naim B, Brumfeld V, Kapon R, Kiss V, Nevo R, Reich Z (2007) J Biol Chem 282:3881–3888
14. Wei XB, Henke VG, Strubing C, Brown EB, Clapham DE (2003) Biophys J 84:1317–1327
15. Keminer O, Peters R (1999) Biophys J 77:217–228
16. Peters R (1983) J Biol Chem 258:11427–11429
17. Ribbeck K, Gorlich D (2001) EMBO J 20:1320–1330
18. Terry LJ, Shows EB, Wente SR (2007) Science 318:1412–1416
19. Gorlich D, Seewald MJ, Ribbeck K (2003) EMBO J 22:1088–1100
20. Timney BL, Tetenbaum-Novatt J, Agate DS, Williams R, Zhang W, Chait BT, Rout MP (2006) J Cell Biol 175:579–593
21. Cardarelli F, Serresi M, Bizzarri R, Beltram F (2008) Traffic 9:528–539
22. Cardarelli F, Serresi M, Bizzarri R, Giacca M, Beltram F (2007) Mol Ther 15:1313–1322
23. Renkin EM (1954) J Gen Physiol 38:225–243
24. Cardarelli F, Bizzarri R, Serresi M, Albertazzi L, Beltram F (2009) J Biol Chem 284:36638–36646
25. Wachter RM, King BA, Heim R, Kallio K, Tsien RY, Boxer SG, Remington SJ (1997) Biochemistry 36:9759–9765
26. Digman MA, Dalal R, Horwitz AF, Gratton E (2008) Biophys J 94:2320–2332
27. Chen Y, MacDonald PJ, Skinner JP, Patterson GH, Muller JD (2006) Microsc Res Tech 69:220–226
28. Terry BR, Matthews EK, Haseloff J (1995) Biochem Biophys Res Commun 217:21–27
29. Arai R, Wriggers W, Nishikawa Y, Nagamune T, Fujisawa T (2004) Proteins 57:829–838
30. Mohr D, Frey S, Fischer T, Guttler T, Gorlich D (2009) EMBO J 28:2541–2553
31. Catimel B, Teh T, Fontes MR, Jennings IG, Jans DA, Howlett GJ, Nice EC, Kobe B (2001) J Biol Chem 276:34189–34198
32. Percipalle P, Butler PJ, Finch JT, Jans DA, Rhodes D (1999) J Mol Biol 292:263–273
33. Cardarelli F, Gratton E (2010) PLoS One 5:e10475
34. Cardarelli F, Lanzano L, Gratton E (2011) Biophys J 101: L27–L29
35. Cardarelli F, Serresi M, Albanese A, Bizzarri R, Beltram F (2011) J Biol Chem 286:12292–12299